Distinct element modelling of the mechanical behavior of intact rocks using Voronoi tessellation model

Mojtaba Bahaaddini [a, *], Mansoreh Rahimi [b]

[a] Shahid Bahonar University of Kerman, Kerman, Iran
[b] Department of mining Engineering, Higher Education Complex of Zarand, Zarand, Iran

ABSTRACT

This paper aims to study the mechanical behavior and failure mechanism of intact rocks under different loading conditions using the grain-based model implemented in the Universal Distinct Element Code (UDEC). The grain-based numerical model is a powerful tool to investigate the complicated micro-structural mechanical behavior of rocks. In the UDEC grain-based model, the intact material is simulated as assemblies of a number of polygonal blocks bonded together at their contact areas. To investigate the ability of such a numerical framework, the uniaxial and triaxial compression tests as well as the direct tensile test were simulated in the UDEC and then the results were compared with that of the laboratory experiments undertaken on the Hawkesbury sandstone. There was a good agreement between the experimental and numerical results under different loading conditions. In order to investigate the effect of micro-properties of the grain-based model, blocks and contacts, on the laboratory scale intact rocks, a set of parametric studies was undertaken. The results from this analysis confirmed that the block size is an intrinsic characteristic of a model which has a significant effect on the mechanical behavior of the numerical models. In addition, it was concluded that cohesion and friction angle of contact surfaces control both the uniaxial and triaxial compressive strengths. Finally, it was found that in the triaxial compression test, as the applied confining pressure increases, the effect of contact cohesion on the strength decreases while the effect of the friction angle increases.

Keywords : Voronoi model; Grain-based model; UDEC; micro-parameters; Failure mechanism

1. Introduction

Mechanical behavior of brittle rocks is primarily controlled by the shape and size distribution of grains, as well as the cementation or matrix (bond) between the grains [1]. Failure mechanism of rocks has been one of the main concerns of rock engineers due to its role in the stability assessment of rock structures. The formation of a failure plane is a result of initiation and propagation of micro-cracks that depends on the inherent mechanical properties and stress distribution among the grains [2]. The bonds between the grains also play an important role in the strength and deformation behavior of rocks [3]. In a micro-scale model, the failure initiates by the generation of small cracks at the boundary of crystalline grains followed by the coalescence of micro-cracks and the rupture of the intact material [4].

Conducting laboratory experiments to understand how grains and bonds control the mechanical behavior of intact materials is problematic due to the difficulties in preparation of specimens with similar grain structures and various cementations even with artificial materials [3]. Since the early 1980s, there has been a significant growth and improvement in numerical models, which have been employed to simulate the initiation and propagation of the failure in rock-like materials.
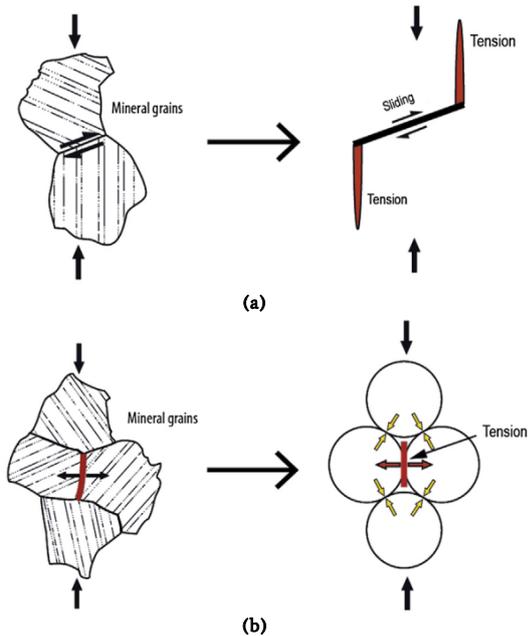
Two approaches are typically used to numerically simulate the failure process including the sliding crack model [5, 6] and the force-chain model [7], as shown in Fig. 1. In the former, the presence of a weak plane is required to occur the sliding before the tensile stresses generate the wing cracks at the tips of the weak planes (Fig. 1a). In the force-chain model, the heterogeneous nature of grain assemblies results in concentration of local tensile stress, which then leads to the breakage of bonds under the tension (Fig. 1b). The sliding crack model indicates that under a compressive loading condition, rocks are weaker in shear than in tension and the sliding should occur first to generate the tensile cracks, while in the force-chain model, the shear fractures develop once a sufficient number of the tensile cracks appears [8]. A review of previous studies clearly shows that the sliding crack model cannot efficiently simulate the early stage cracking process of rock-like materials and the measured crack initiation and growth in rock materials supports the concept of the force-chain model [2, 7-9].

Recent developments in the Discrete Element Method (DEM) and the computer technology have led to revolutionary advancement in understanding the complex failure mechanism of rock-like materials. DEM involves all modelling techniques that treat the materials as separate bodies that are allowed to displace or rotate, and are also able to automatically recognize the new contacts in the simulation process [11]. Two commercial DEM codes of Universal Distinct Element Code (UDEC) and Particle Flow Code (PFC) have been widely used to simulate the mechanical behavior of rock materials. In PFC, the intact material is simulated as assemblies of circular (2D) or spherical (3D) particles bonded together at contact points, called Bonded Particle Model (BPM). BPM has shown promising results in reproducing many mechanical features of rocks in laboratory and large-scale experiments [12-18]. However, BPM suffers from underestimation of the tensile strength and the slope of failure envelope [7, 19, 20]. To resolve these issues, many attempts have been undertaken, such as reducing the size of particles and refining the particles shape by clustering [7] or by clumping [9, 21], changing the particle size distribution and reducing

---

* Corresponding author Tel: +983432121003, Fax: +983432112764. *E-mail address:* mojtaba_bahaaddini@yahoo.com (M. Bahaaddini).

the porosity [22] and applying the grain-based model (GBM) [23]. However, challenges still remain.
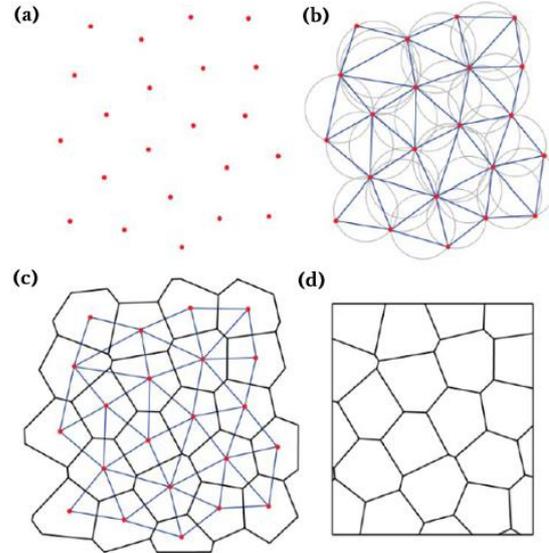

Fig.1. Models for cracking simulation of heterogeneous assemblies of grains: a) Sliding crack model and b) Force chain crack model [10].

Implementation of the Voronoi tessellation generator in UDEC has been a major improvement in efficient simulation of a polygonal structure of intact materials. In this method, the intact material is partitioned into polygons with a pre-defined edge length and size distribution. These polygons represent the mineral grains, which are bonded together. These grains are not breakable and the failure occurs at the polygonal boundaries. The force-displacement relationship between the grains follows the same rules as that of BPM with exception of the bonding at contacts area as opposed to the point-type contacts in BPM.

This paper aims to investigate the ability of the Voronoi model in reproducing the mechanical behavior of the Hawkesbury sandstone under different loading regimes. To this end, the direct tensile, and the uniaxial and triaxial compressive tests were simulated using the Voronoi model and the results were compared against the laboratory data. In the Voronoi model, the mechanical behavior of materials is controlled by micro-properties of the grains and bonds. To assess how these micro-properties control the macro-scale response of the materials, a parametric study on these parameters was then undertaken.

2. UDEC grain-based model

As noted earlier, the micro-structure in the Voronoi model is simulated as the assemblies of a number of distinct deformable or rigid polygons. An automatic built-in Voronoi generator has been implemented in UDEC, where a specified region in the model can be sub-divided into randomly sized polygons. The logic of the Voronoi tessellation algorithm is shown schematically in Fig. 2. In this algorithm, a set of points is randomly distributed within the tessellation region (Fig. 2a). These points are allowed to move in the iteration procedure. The user specifies an iteration number to control the uniformity of the spacing between the points. A greater number of iteration leads to a more uniform tessellation. Triangles are created between all points and each triangle is circumscribed within a circle containing triangular vertices, called the Delaunay triangulation (Fig. 2b). Afterwards, bisectors of all triangles that share a common side are constructed to form the Voronoi polygons (Fig. 2c). Finally, these polygons are truncated at the boundary of the model (Fig. 2d) [24, 25].

Fig. 2. Voronoi tessellation generator logic used in UDEC: (a) Random generation of points, (b) Creation of the Delaunay triangulation, (c) Generation of the Voronoi blocks and (d) Truncation of polygons at the boundary of the tessellation region [24].

The mechanical behavior of the Voronoi model is controlled by micro-properties of blocks and contact areas, as shown in Fig. 3. Each Voronoi polygon is subdivided into finite difference zones and obeys the isotropic elastic deformable model. The deformability of blocks is controlled by micro-properties of bulk modulus (K) and shear modulus (G). The Voronoi contacts follow the Coulomb sliding area model, as shown in Fig. 4. The micro-scale properties of the Voronoi contacts consists of normal stiffness (k_n), shear stiffness (k_s), cohesion (c), friction angle (ϕ) and tensile strength (σ_t). The force-displacement relationship in the normal direction is assumed to be linear and is controlled by the normal stiffness according to:

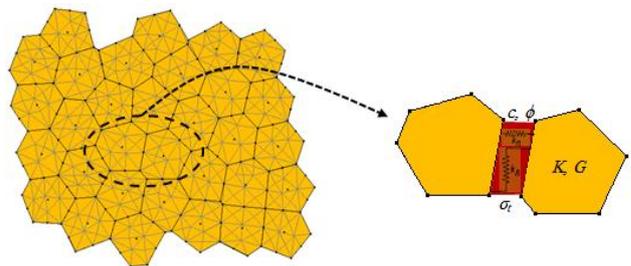$$\Delta\sigma_n = -k_n \Delta u_n \tag{1}$$

Where $\Delta\sigma_n$ is the effective normal stress increment and Δu_n is the normal displacement increment. When the applied normal stress exceeds the tensile strength ($\sigma_n < -\sigma_t$), the bond breaks under the tension where the tensile strength is reduced to zero. The movement of particles toward each other leads to the particles overlap, as shown in Fig. 4.

The shear strength of bond τ_{max} is determined by the contact properties of c and ϕ as follows:

$$\left|\tau_s\right| \le c + \sigma_n \tan\phi = \tau_{max} \tag{2}$$

When the shear stress is lower than the shear strength, the response of the Voronoi contacts is controlled by the shear stiffness based on:

$$\Delta\tau_s = -k_s \Delta u_s^e \tag{3}$$

Fig. 3. Micro-parameters of UDEC grain-based model.

Where $\Delta\tau_s$ is the effective shear stress increment and Δu_s^e is the elastic component of incremental shear displacement. When the shear stress exceeds the shear strength ($\left|\tau_s\right| \ge \tau_{max}$), the bond breaks and the sliding occurs along the shear crack [3, 26].

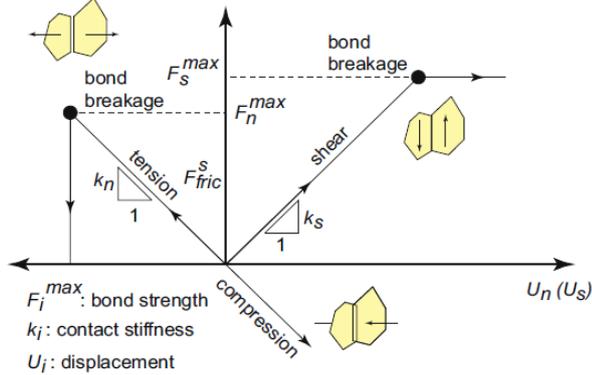$$\tau_s = sign(\Delta u_s^e)\tau_{max} \qquad (4)$$

Fig. 4. The Coulomb contact slip model [27, 28].

3. Simulation of the mechanical behavior of the Hawkesbury sandstone

This section investigates the ability of the Voronoi modelling in reproducing the mechanical behavior of rocks under different loading regimes. The results of experimental tests on the Hawkesbury sandstone were used for this purpose. The Hawkesbury sandstone forms the bedrock of Sydney region, Australia, and many civil and mining structures have been constructed in or on this bedrock [29-31].

3.1. Modelling procedure

Numerical specimens having a width of 50 mm and a height of 100 mm were generated and the uniaxial and triaxial compression tests as well as the direct tensile test were simulated. A schematic illustration of the uniaxial compression test simulation is shown in Fig. 5. In the uniaxial compression test, a velocity of 0.01 m/s was applied to the upper and lower boundaries of the model, and the applied axial stress was measured during the loading process. Preliminary study showed that this velocity rate is low enough to ensure that the specimen fails in a quasi-static condition. Four measurement points were placed at the top and bottom of the specimen and the axial strain was recorded during the loading process by dividing the measured axial deformation to the length of specimen. The lateral strain was recorded by measuring the horizontal displacement of the measurement points, which were placed

at the left and right sides of the specimen.

In the triaxial compression test, a constant normal stress was applied to the left and right boundaries of the model during the loading process. In the direct tensile test, the velocity boundary conditions were applied in the opposite direction for applying the uniaxial tensile loading.
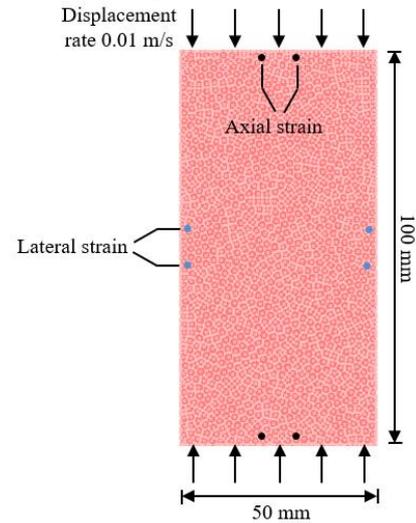

Fig. 5. Simulation of the uniaxial compression test.

3.2. Micro-parameters calibration

The micro-parameters, referred above, cannot be measured in a laboratory and needs to be determined through the calibration process. Calibration is an iterative process to reproduce the mechanical properties of intact rock measured from laboratory experiments [19].

In the calibration process, first, the grain size should be chosen. The grain size should be small enough to ensure that the macro-scale fracture coalescence is independent of the geometries of the Voronoi blocks [32]. Then, the Poisson's ratio is calibrated that is dependent on elastic properties of the deformable block (K and G) and contact stiffness ratio (k_n/k_s). Once the contact stiffness ratio has been set, the contact's normal stiffness and shear stiffness are calibrated to reproduce the Elastic modulus. In the final stage, the contact strength properties are calibrated to recover the strength properties measured in the laboratory [33, 34]. The calibrated micro-properties are presented in Table 1.

Table 1. Calibrated micro-scale properties.

Block parameters				Contact parameters				
Density (kg/m³)	Size (mm)	Bulk modulus (GPa)	Shear modulus (GPa)	Normal stiffness (GPa/mm)	Shear stiffness (GPa/mm)	Cohesion (MPa)	Friction angle (Deg.)	Tensile strength (MPa)
2650	2	5	2	15	6.8	7.5	25	2.5

3.3. Validation study

The stress-strain curve of the numerical model under the uniaxial compression test is shown in Fig. 6. The sample failed in the brittle mode having a good agreement with experimental results (Fig. 7). The generation and coalescence of tensile cracks along the vertical axis of specimens was the failure mechanism in both experimental and numerical cases, which was then followed by the development of a steep plane and its concurrent sliding.

The triaxial compression tests were undertaken at different confining pressures ranging from 1 to 10 MPa and the results are shown in Figs 8 and 9. As the confining pressure increases, the peak strength increases and the post-peak behavior transits from a brittle regime to a ductile one. Increasing the confining pressure also alters the failure mode, as shown in Fig. 9. Increasing the confining pressure results in a reduction of tensile cracks initiation and propagation in which the failure occurred

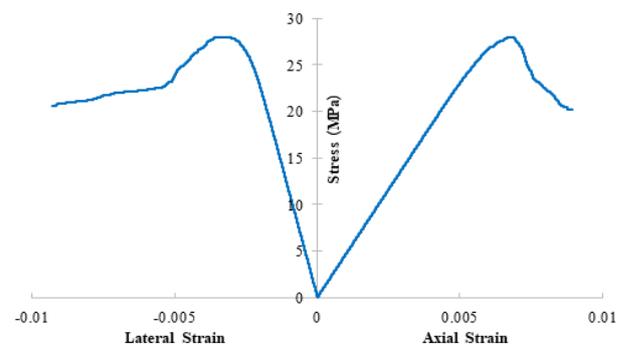through the creation and sliding along a shear plane.

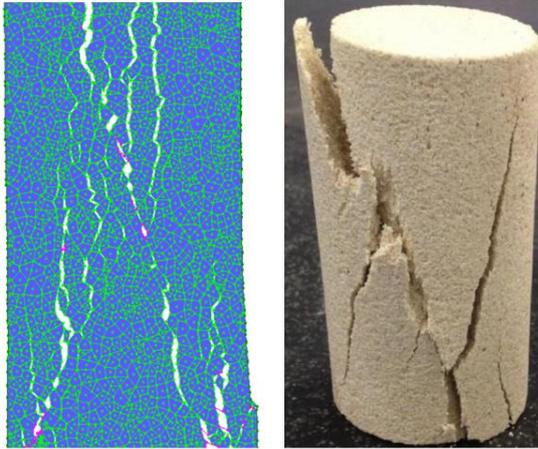**Fig. 6.** Stress-strain curve of the calibrated numerical model.

Fig. 7. Comparison of the failure modes resulted from numerical model and experimental test under the uniaxial compression.
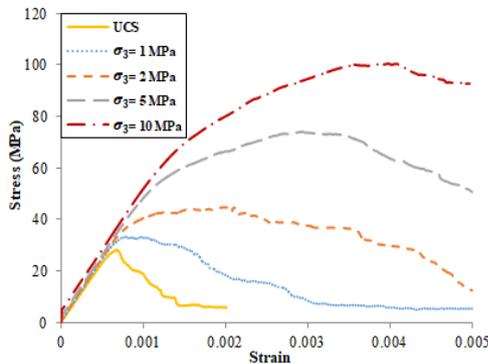

Fig. 8. Effect of confining pressure on the stress-strain curve in the voronoi model.

The strength of the Voronoi models under different loading regimes are compared against the measured experimental tests in Fig. 10 (the deviations of experimental tests are shown by error bars). These results clearly show that the Voronoi model can properly reproduce the strength of material under different loading conditions. Since the shape

of grains in the Voronoi model is polygonal, the interlocking between the particles and the resistance against the rotation of grains takes place and leads to a suitable reproduction of the failure envelope, while in the PFC model due to circular shape of particles, the reproduction of the failure envelope is not feasible.
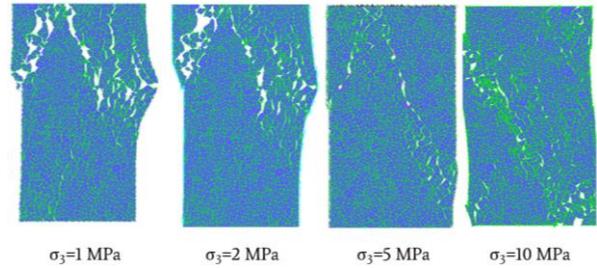

$\sigma_3=1$ MPa $\sigma_3=2$ MPa $\sigma_3=5$ MPa $\sigma_3=10$ MPa

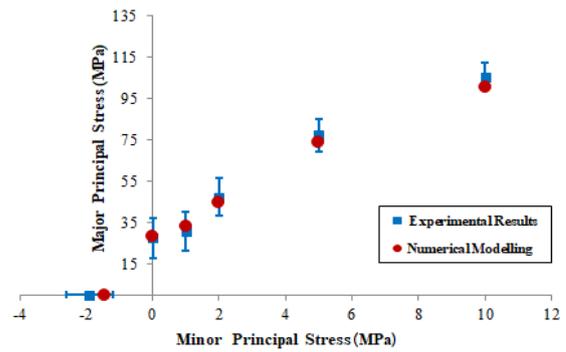**Fig. 9.** Effect of confining pressure on the failure mode in the voronoi model.

Fig. 10. Comparison of the results of numerical model and experimental tests under different loading regimes.

The results from numerical simulations of the uniaxial compression test, the direct tensile test and the triaxial compression tests are presented in Table 2 and they are compared against the experimental tests on the Hawkesbury sandstone. It can be seen that the numerical results are in good agreement with the laboratory data. These results clearly show that the Voronoi model is able to reproduce the mechanical behavior of intact materials under different loading conditions.

Table 2. Comparison of the results of numerical and experimental tests.

Experiment	Uniaxial compression test			Direct tensile test	Triaxial compression test			
					Mohr-Coulomb		Hoek-Brown	
Parameter	UCS (MPa)	E (GPa)	ν	σ_t (MPa)	c (MPa)	φ (Deg.)	m_i	σ_{ci} (MPa)
Experimental test	27.4	4.2	0.2	1.9	4.9	50.6	30	27.4
Numerical modelling	28.03	4.36	0.23	1.44	5.32	50.3	30.3	24.7

4. Parametric study

As noted earlier, the mechanical behavior of the Voronoi model is controlled by micro-properties of the Voronoi blocks and contact areas. These parameters cannot be measured in the laboratory and must be determined through the calibration process. Therefore, it is of great importance to understand how these micro-parameters affect the macro-scale mechanical behavior of models.

4.1. Block parameters

4.1.1. Voronoi block size

To investigate the effect of the Voronoi block's size on the mechanical behavior of numerical models, the Voronoi edge's length varied from 2 mm to 20 mm where other micro-properties were kept constant (Table 1). Uniaxial compression, triaxial compression at 5 MPa confining

pressure and direct tensile tests were carried out and the results are shown in Fig. 11. In order to present the effect of the Voronoi size on the strength at different loading conditions, the measured strengths were normalized to the corresponding calibrated value reported in Table 2. As the block size increases, the strength of the material at different loading conditions increases. The increment of the block size results in increment increases the Elastic modulus and decreases the Poisson's ratio. These findings are in agreement with previous studies, as well [24, 35]. As the intact material is simulated by the well-connected polygonal blocks, the Voronoi model is not naturally able to simulate the voids and intrinsic micro-cracks of the intact material. As the block size increases, the total number of the Voronoi blocks in numerical specimen decreases in which the mechanical behavior of the material is largely controlled by the blocks than the contact areas. As these blocks are assumed elastic and the failure only takes place at the boundary of these blocks, increasing the block size results in increasing the strength and alteration of the failure mechanism. Therefore, the block size is not just a parameter that controls the resolution of material, but also it is an

intrinsic characteristic of the model that has a significant effect on the mechanical behavior of the model [32, 36, 37].
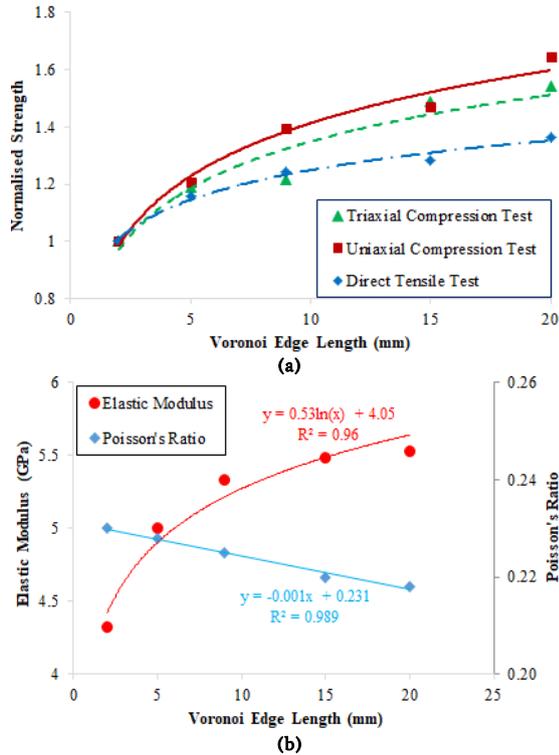

Fig. 11. Effect of the Voronoi block size on: (a) normalized direct tensile, uniaxial and triaxial compressive strengths, (b) Elastic modulus and Poisson's ratio.

4.1.2. Bulk modulus of blocks

The bulk modulus of the Voronoi blocks was varied in the range of 3.5 to 6.5 GPa in which the other parameters were kept constant. The uniaxial compression tests were undertaken and the results are presented in Fig. 12. The bulk modulus has no significant effect on the strength while the increase in bulk modulus leads to an increase in Elastic modulus as well as a decrease in the Poisson's ratio.
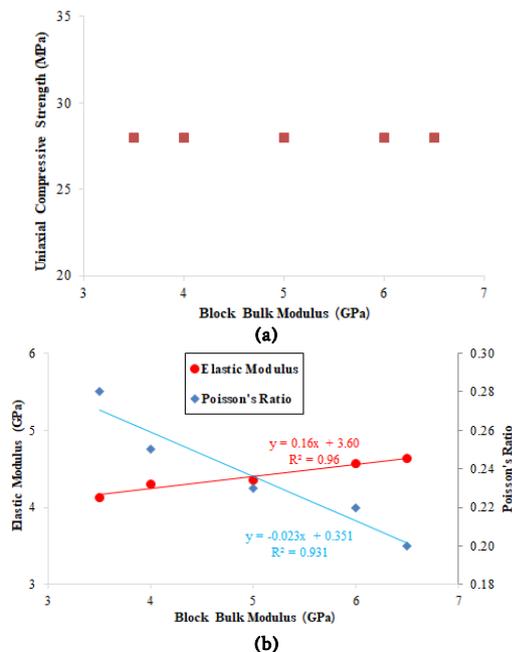

Fig. 12. Effect of block bulk modulus on: (a) uniaxial compressive strength and (b) Elastic modulus and Poisson's ratio.

4.1.3. Shear modulus of blocks

The effect of shear modulus of blocks was investigated by varying this parameter from 1 to 3.5 GPa whilst the other micro-properties were kept constant. As shown in Fig. 13, the increase in shear modulus results in an increase in the Elastic modulus and a decrease in the Poisson's ratio while this parameter has no effect on the strength.
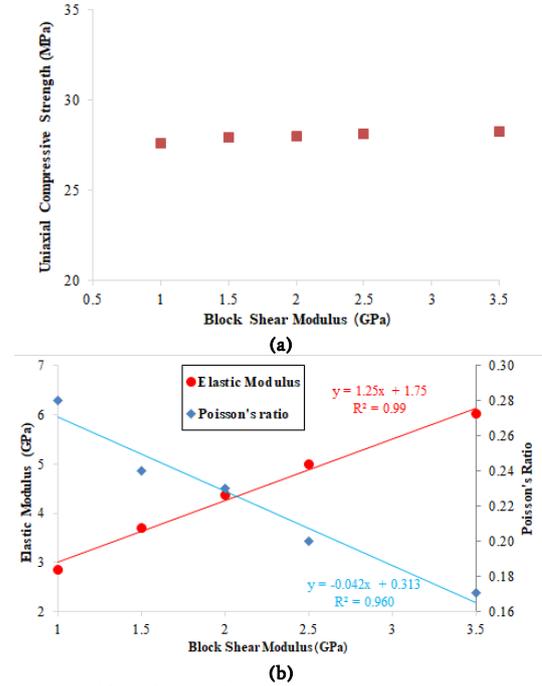

Fig. 13. Effect of block shear modulus on: (a) uniaxial compressive strength and (b) Elastic modulus and Poisson's ratio.

4.2. Contact parameters

4.2.1. Contact Normal stiffness

To investigate the effect of the contact normal stiffness on the mechanical behavior of the numerical models, the contact normal stiffness was varied from 8 to 25 GPa/mm with constant contact stiffness ratio ($k_n/k_s = 2.2$). The results are shown in Fig. 14. As the contact normal stiffness increases, the Elastic modulus increases and the Poisson's ratio slightly decreases. This parameter revealed no effect on the strength of the specimens.

4.2.2. Contact stiffness ratio

To consider the effect of the contact stiffness ratio (k_n/k_s) on the mechanical behavior of a grain-based model, the contact stiffness ratio varied from 1.2 to 3.7 (with constant shear stiffness) in which the other micro-properties were kept constant. The results (depicted in Fig. 15) show that the contact stiffness ratio had no significant effect on the strength while the increase in contact stiffness ratio led to an increase in Elastic modulus and a decrease in the Poisson's ratio.

4.2.3. Contact cohesion

The effect of the contact cohesion on strength of the model at different loading conditions was investigated by changing this parameter in the range of 6 to 9 MPa where other parameters were kept constant (Table 1). The contact cohesion showed no obvious effect on the tensile strength while the increase in this parameter led to an increase in uniaxial and triaxial compressive strengths (Fig. 16). It is noteworthy that the impact of the contact cohesion on the triaxial strength decreases with an increase in the applied confining pressure.
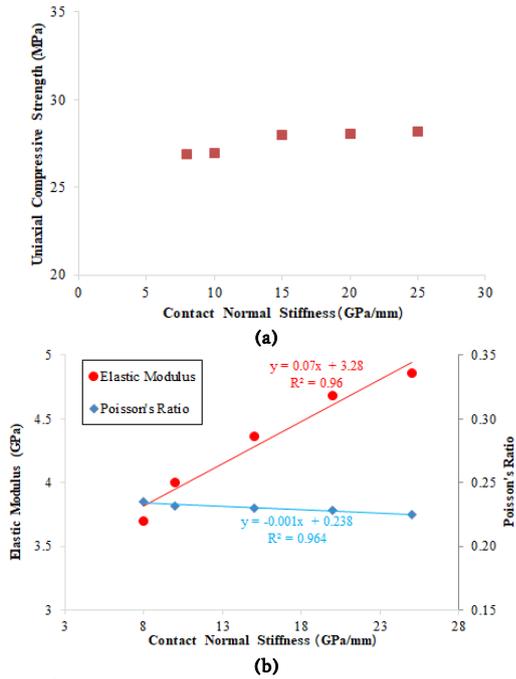
Fig. 14. Effect of contact normal stiffness on: (a) uniaxial compressive strength and (b) Elastic modulus and Poisson's ratio.

Fig. 15. Effect of contact stiffness ratio on: (a) uniaxial compressive strength and (b) Elastic modulus and Poisson's ratio.

4.2.4. Contact friction angle

The effect of contact friction angle on the strength of the models under different loading conditions is shown in Fig. 17. The friction angle varied from 15 to 35 degrees and other micro-parameters were kept constant. The contact friction angle has no effect on the tensile strength while the increase in contact friction led to an increase in uniaxial and triaxial compressive strengths. It is interesting to note that unlike the contact cohesion, when the confining pressure increases, the impact of the contact friction angle on the triaxial compressive strength increases.
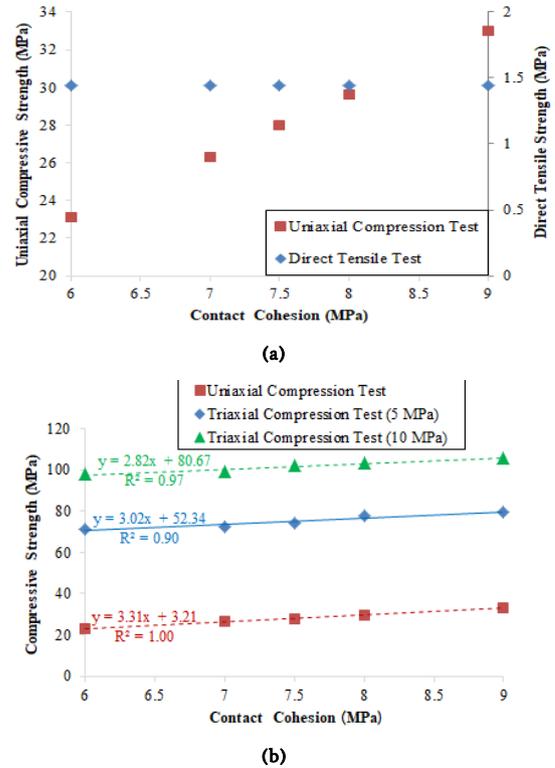

Fig. 16. Effect of contact cohesion on: (a) uniaxial compressive strength and direct tensile strength (b) Triaxial compressive strength at different confining pressure.
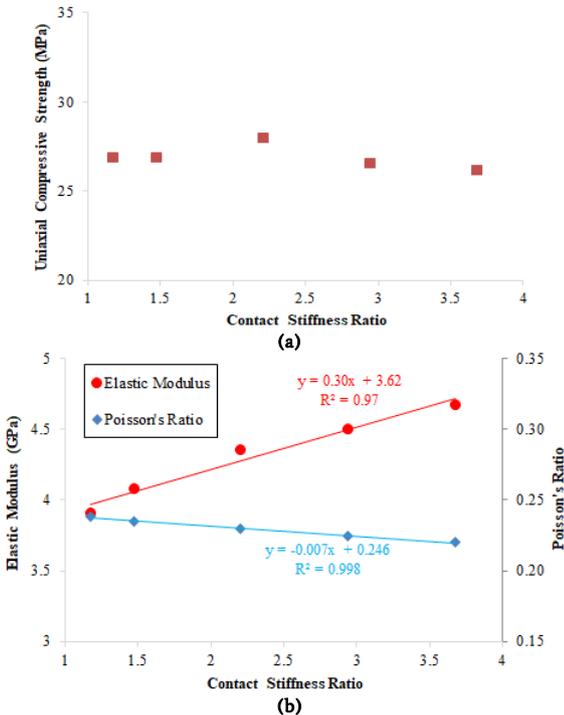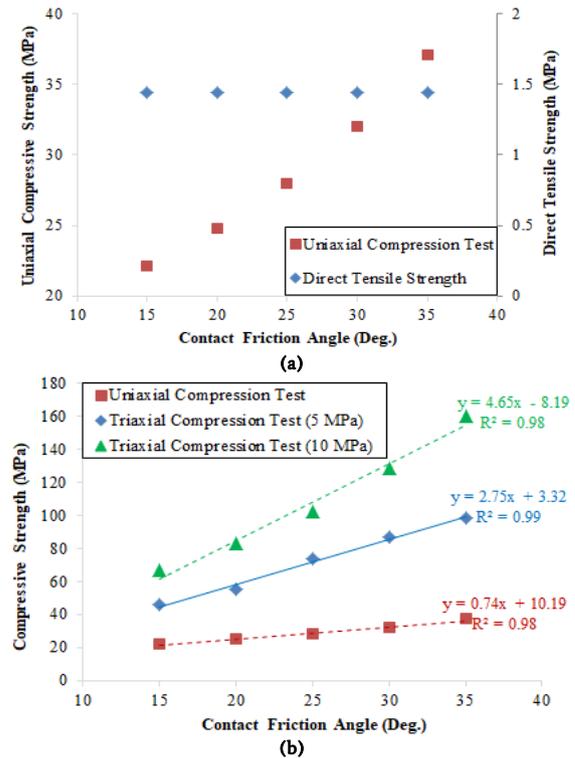

Fig. 17. Effect of contact friction angle on: (a) uniaxial compressive strength and direct tensile strength (b) Triaxial compressive strength at different confining pressure.

4.2.5. Contact tensile strength

To investigate the effect of the contact tensile strength on the mechanical behavior of the Voronoi model, this parameter was changed

in the range of 1 to 4 MPa and the results are presented in Fig. 18. The increase in contact tensile strength results in an increase in both uniaxial compressive and tensile strengths. However, the impact of the contact tensile strength on the triaxial compressive strength diminishes with an increase in confining pressure.
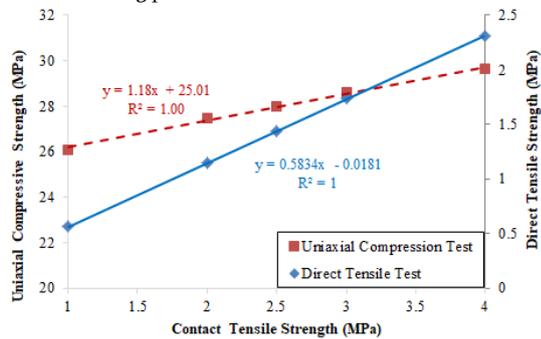

Fig. 18. Effect of contact tensile strength on the uniaxial compressive and direct tensile strength.

5. Conclusions

In this study, the mechanical behavior of an intact material was simulated using the Voronoi tessellation method. The uniaxial and triaxial compression and direct tensile tests were simulated using the UDEC code and the results were compared against the experimental data obtained from the Hawkesbury sandstone. It was found that unlike the bonded particle model in PFC, the Voronoi model can reproduce the strength of the material under different loading conditions. Since, the mechanical behavior of the Voronoi models is controlled by the micro-properties of the blocks and the contact areas, a parametric study was undertaken to understand how these micro-properties control the macro-scale behaviors. The results showed that the Elastic modulus of the material is directly related to the bulk and shear modulus of the blocks, the contact normal stiffness and the contact stiffness ratio. The tensile strength of the material is only dependent on the contact tensile strength. The uniaxial compressive strength of the material is linearly dependent on contact cohesion, friction angle and tensile strength. It was found that in the triaxial compression test with an increase in the confining pressure, the influence of the contact friction angle on the strength increases while the impact of contact cohesion and tensile strength diminishes. Studying the effect of the Voronoi block size showed that as the size of the Voronoi blocks increases, the strength of the material under different loading condition increases. Since the intact material is simulated by well-connected polygons, the voids and micro-cracks are not simulated in the Voronoi model and by increasing the block size, the mechanical behavior of the model is controlled by the blocks properties than the contact areas.

REFRENCES

[1] Delenne, J. Y., Soulié, F., El Youssoufi, M. S. & Radjai, F. (2011). Compressive strength of an unsaturated granular material during cementation. Powder Technology, 208(2), 308-11. http://dx.doi.org/10.1016/j.powtec.2010.08.021

[2] Nicksiar, M. & Martin, C. D. (2013). Crack initiation stress in low porosity crystalline and sedimentary rocks. Engineering Geology, 15464-76. http://dx.doi.org/10.1016/j.enggeo.2012.12.007

[3] Gao, F. & Kang, H. (2017). Grain-Based Discrete-Element Modeling Study on the Effects of Cementation on the Mechanical Behavior of Low-Porosity Brittle Rocks. International Journal of Geomechanics, 17(9), 04017061. doi:10.1061/(ASCE)GM.1943-5622.0000957

[4] Nicksiar, M. & Martin, C. D. (2014). Factors Affecting Crack Initiation in Low Porosity Crystalline Rocks. Rock Mechanics and Rock Engineering, 47(4), 1165-81. 10.1007/s00603-013-0451-2

[5] Nemat-Nasser, S. & Horii, H. (1982). Compression-induced nonplanar crack extension with application to splitting, exfoliation, and rockburst. Journal of Geophysical Research, 87(B8), 6805-21.

[6] Nemat-Nasser, S. & Obata, M. (1988). A Microcrack Model of Dilatancy in Brittle Materials. Journal of Applied Mechanics, 55(1), 24-35. 10.1115/1.3173647

[7] Potyondy, D. O. & Cundall, P. A. (2004). A bonded-particle model for rock. International Journal of Rock Mechanics & Mining Sciences, 41(8), 1329-64. 10.1016/j.ijrmms.2004.09.011

[8] Nicksiar, M. (2013). Effective parameters on crack initiation stress in low porosity rocks. PhD Thesis, University of Alberta, Edmonton, Alberta.

[9] Cho, N. (2008). Discrete element modeling of rock pre-peak fracturing and dilation. PhD Thesis, University of Alberta, Edmonton, Alberta.

[10] Hoek, E. & Martin, C. D. (2014). Fracture initiation and propagation in intact rock – A review. Journal of Rock Mechanics and Geotechnical Engineering, 6(4), 287-300. http://dx.doi.org/10.1016/j.jrmge.2014.06.001

[11] Cundall, P. A. & Hart, R. D. (1992). Numerical modeling of discontinua. Engineering Computations, 9(2), 101-13.

[12] Bahaaddini, M., Sharrock, G. & Hebblewhite, B. K. (2013). Numerical direct shear tests to model the shear behaviour of rock joints. Computers and Geotechnics, 51101-15. http://dx.doi.org/10.1016/j.compgeo.2013.02.003

[13] Bahaaddini, M., Hagan, P. C., Mitra, R. & Khosravi, M. H. (2016). Experimental and numerical study of asperity degradation in the direct shear test. Engineering Geology, 20441-52.

[14] Bahaaddini, M., Hagan, P. C., Mitra, R. & Hebblewhite, B. K. (2014). Scale effect on the shear behaviour of rock joints based on a numerical study. Engineering Geology, 181212-23. http://dx.doi.org/10.1016/j.enggeo.2014.07.018

[15] Bahaaddini, M., Hagan, P. C., Mitra, R. & Hebblewhite, B. K. (2016). Numerical study of the mechanical behaviour of non-persistent jointed rock masses. International Journal of Geomechanics, 16(1), 040150351-10. DOI: 10.1061/(ASCE)GM.1943-5622.0000510.

[16] Mas Ivars, D., Pierce, M. E., Darcel, C., Reyes-Montes, J., Potyondy, D. O., Young, R. P., et al. (2011). The synthetic rock mass approach for jointed rock mass modelling. International Journal of Rock Mechanics & Mining Sciences, 48(2), 219-44. 10.1016/j.ijrmms.2010.11.014

[17] Hadjigeorgiou, J., Esmaieli, K. & Grenon, M. (2009). Stability analysis of vertical excavations in hard rock by integrating a fracture system into a PFC model. Tunnelling and Underground Space Technology, 24(3), 296-308. 10.1016/j.tust.2008.10.002

[18] Esmaieli, K., Hadjigeorgiou, J. & Grenon, M. (2010). Estimating geometrical and mechanical REV based on synthetic rock mass models at Brunswick Mine. International Journal of Rock Mechanics & Mining Sciences, 47(6), 915-26.

[19] Bahaaddini, M., Sharrock, G. & Hebblewhite, B. K. (2013). Numerical investigation of the effect of joint geometrical parameters on the mechanical properties of a non-persistent jointed rock mass under uniaxial compression. Computers and Geotechnics, 49, 206-25. http://dx.doi.org/10.1016/j.compgeo.2012.10.012

[20] Potyondy, D. O. (2015). The bonded-particle model as a tool for rock mechanics research and application: current trends

and future directions. Geosystem Engineering, 18(1), 1-28. 10.1080/12269328.2014.998346

[21] Cho, N., Martin, C. D. & Sego, D. C. (2007). A clumped particle model for rock. International Journal of Rock Mechanics & Mining Sciences, 44(7), 997-1010. 10.1016/j.ijrmms.2007.02.002

[22] Schöpfer, M. P. J., Abe, S., Childs, C. & Walsh, J. J. (2009). The impact of porosity and crack density on the elasticity, strength and friction of cohesive granular materials: Insights from DEM modelling. International Journal of Rock Mechanics & Mining Sciences, 46(2), 250-61. 10.1016/j.ijrmms.2008.03.009

[23] Potyondy, D. O. (2011). Parallel-Bond Refinements to Match Macroproperties of Hard Rock. 2nd International FLAC/DEM Symposium, Melbourne.

[24] Fabjan, T., Mas-Ivars, D. & Vukadin, V. (2015). Numerical simulation of intact rock behaviour via the continuum and Voronoi tesselletion models − a sensitivity analysis. Acta Geotechnica Slovenica, 2015(2), 5-23.

[25] Itasca Consulting Group. Inc. UDEC (Universal Distinct Element Code) user's manual. Minneapolis, Minnesota2014.

[26] Kazerani, T. & Zhao, J. (2010). Micromechanical parameters in bonded particle method for modelling of brittle material failure. International Journal for Numerical and Analytical Methods in Geomechanics, 34(18), 1877-95.

[27] Kazerani, T. (2011). Micromechanical study of rock fracture and fragmentation under dynamic loads using discrete element method. PhD Thesis, LMR Laboratoire de mécanique des roches, Suisse.

[28] Lisjak, A. & Grasselli, G. (2014). A review of discrete modeling techniques for fracturing processes in discontinuous rock masses. Journal of Rock Mechanics and Geotechnical Engineering, 6(4), 301-14. http://dx.doi.org/10.1016/j.jrmge.2013.12.007

[29] Masoumi, H., Horne, J. & Timms, W. (2017). Establishing Empirical Relationships for the Effects of Water Content on the Mechanical Behavior of Gosford Sandstone. Rock Mechanics and Rock Engineering, 50(8), 2235-42.

10.1007/s00603-017-1243-x

[30] Sharrock, G. B., Akram, M. S. & Mitra, R. (2009). Application of synthetic rock mass modeling to estimate the strength of jointed sandstone. 43rd US Rock Mechanics Symposium & 4th US - Canada Rock Mechanics Symposium, Asheville, North Carolina.

[31] Roshan, H., Masoumi, H., Zhang, Y., Al-Yaseri, A. Z., Iglauer, S., Lebedev, M., et al. (2017). Micro-structural effects on mechanical properties of Shaly-sandstone. , . Journal of Geotechnical and Geoenvironmental Engineering, DOI: 10.1061/(ASCE)GT.1943-5606.0001831.

[32] Gao, F. Q. & Stead, D. (2014). The application of a modified Voronoi logic to brittle fracture modelling at the laboratory and field scale. International Journal of Rock Mechanics and Mining Sciences, 681-14. http://dx.doi.org/10.1016/j.ijrmms.2014.02.003

[33] Mayer, J. M. & Stead, D. (2017). Exploration into the causes of uncertainty in UDEC Grain Boundary Models. Computers and Geotechnics, 82110-23. http://dx.doi.org/10.1016/j.compgeo.2016.10.003

[34] Mayer, J. M. (2015). Applications of uncertainty theory to rock mechanics and geotechnical mine design. MSc Thesis, Simon Fraser University, Burnaby, British Columbia, Canada

[35] Gui, Y. L., Zhao, Z. Y., Ji, J., Wang, X. M., Zhou, K. P. & Ma, S. Q. (2016). The grain effect of intact rock modelling using discrete element method with Voronoi grains. Géotechnique Letters, 6(2), 136-43. 10.1680/jgele.16.00005

[36] Azocar, K. D. (2016). Investigating the mesh dependency and upscaling of 3D grain-based models for the simulation of brittle fracture processes in low-porosity crystalline rock. MSc. Thesis, Queen's University, Kingston, Ontario, Canada.

[37] Ghazvinian, E., Diederichs, M. S. & Quey, R. (2014). 3D random Voronoi grain-based models for simulation of brittle rock damage and fabric-guided micro-fracturing. Journal of Rock Mechanics and Geotechnical Engineering, 6(6), 506-21. http://dx.doi.org/10.1016/j.jrmge.2014.09.001